JOURNAL OF MATERIALS SCIENCE 28 (1993) 6147–6154

Microstructural evolution during liquid-phase sintering of high-speed steel-based composites containing TiN-coated Al_2O_3, TiC, or Al_2O_3 particles: influence on wear properties

C. JOUANNY-TRÉSY*, M. VARDAVOULIAS, M. JEANDIN
Ecole des Mines de Paris, Centre des Matériaux P. M. Fourt, BP87, 91003 Evry, France

A high-speed steel containing 10 vol% TiN-coated Al_2O_3, Al_2O_3, or TiC particles was liquid-phase sintered with the addition of copper–phosphorus. The mixtures were sintered in a furnace with a controlled axial temperature gradient, and their microstructural evolution during sintering was studied using quantitative image analysis. Additional samples were fully densified and tested using a pin-on-disc tribometre. Interfaces were characterized by transmission electron microscopy. The final microstructure depended on the behaviour of the liquid phases surrounding the ceramic particles during sintering, which was different for the three types of particles used, and influenced the wear resistance.

1. Introduction

Excellent wear-resistant materials have been obtained by adding ceramic particles to steels [1–6] or high-speed steels (HSS) matrices which contained 10–20 vol % precipitated carbides [7–11].

Materials fabricated using powder metallurgy are known to have a fine and isotropic microstructure which generally produces good mechanical properties. Ceramic particulate reinforcement may further improve wear resistance. In this study ceramic particles were added to AISI M3 type 2 high-speed steel (M3/2) sintered with a copper–phosphorus addition which induced the formation of liquid phases during sintering. This activated sintering decreases the densification temperature, and thus reduces the production costs (conventional continuous sintering furnaces may be used).

Densification mechanisms of the matrix, M3/2 + Cu_3P, have already been studied [12–15]. The addition of ceramics to this matrix led to very different microstructures depending on the type of ceramics: some of them partly (WC, Mo_2C, etc.) or completely dissolved (SiC, etc.) [16], others reacted only slightly with the matrix (TiC, TiN, etc.) or were inert (Al_2O_3) [17]. In addition to differential thermal analysis (DTA) the microstructural evolution during sintering of selected mixtures was studied using samples sintered in a furnace with a controlled axial temperature gradient. This furnace was formerly designed and developed at the Centre des Matériaux P. M. Fourt, for quenching studies after directional solidification [18], and was more recently used to study the liquid-phase sintering of nickel-based alloys, and high-speed steels [13, 19].

To establish the influence of microstructural parameters on wear properties, pin-on-disc tests were carried out on fully densified materials characterized previously by quantitative image analysis (QIA).

2. Materials and methods

2.1. Powders

The chemical composition of M3/2 powder is given in Table I. The mean particle size was 50 μm, and the shape very intricate, because of their production by water atomization (Fig. 1). This powder was annealed in hydrogen.

The Cu_3P particles were acicular, with a mean particle size of 26 μm (Fig. 1a). The phosphorus content of this powder was 14.8 wt %.

Two types of ceramic particles were added.

(i) particles selected because of their limited reactivity with the matrix, but which seemed to have a quite good wettability by the liquid phases during sintering [1, 20]: TiN-coated Al_2O_3 and TiC powders;

(ii) particles which did not react with the matrix, and were not wet by the liquid metals: Al_2O_3.

TiN coating of Al_2O_3 powder was obtained by chemical vapour deposition (CVD) on a fluidized bed of particles. The characterization procedure of these particles and results (coating thicknesses, etc.) were published previously [21]. The same starting batch of alumina was used (mean grain size 50 μm) for both coated and uncoated powders (Fig. 1). The characteristics of ceramic powders used are showed in Table II.

* *Present address*: ALTRAN Technologies, 58 Bel Gouvion St. Cyr, 75017 Paris

0022–2461

TABLE I Chemical composition (wt %) of the M3/2 powder

C	Mo	W	Cr	V	Si	Mn	Fe	O
1.11	6.26	5.0	3.77	2.68	0.30	0.11	Bal.	0.094

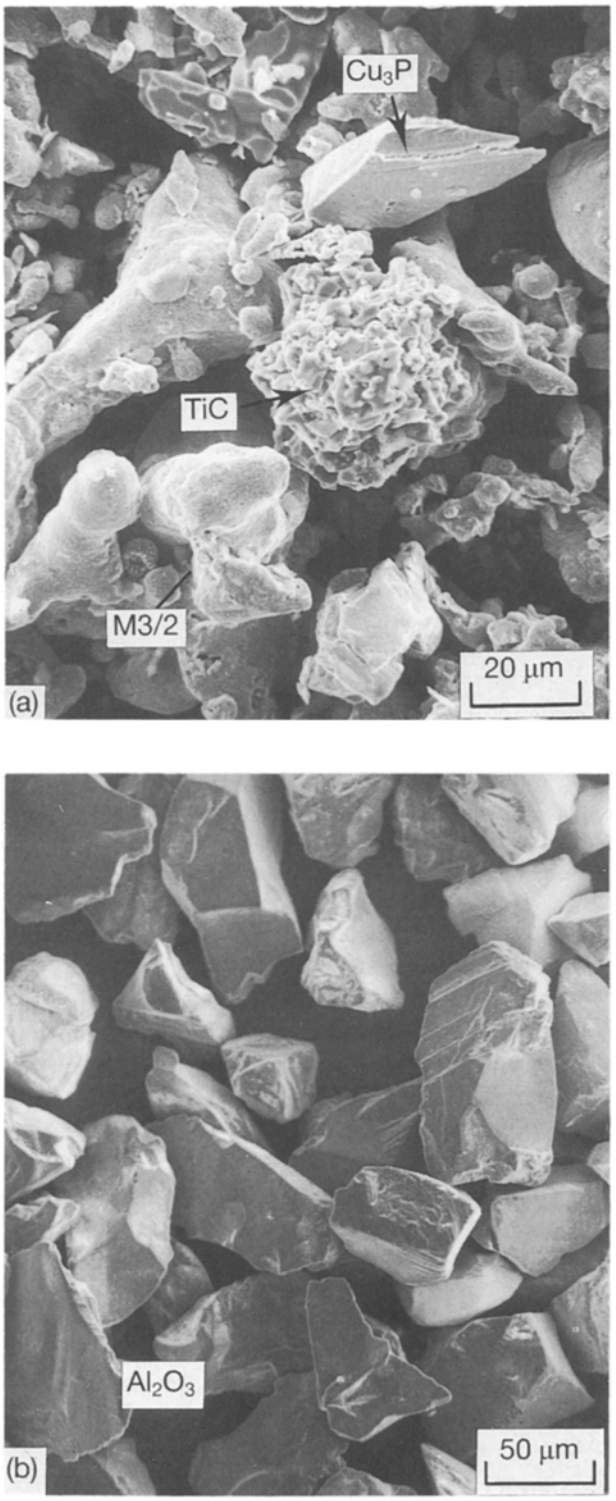

Figure 1 SEM image of powder mixtures before sintering. (a) (M3/2 + 7 wt % Cu_3P + 0.25 wt % C) + 10 vol % TiC. (b) Al_2O_3.

2.2. Sintering

The cupro-phosphorus and carbon contents to be added to the matrix, i.e. 7 wt % Cu_3P and 0.25 wt % C, were determined in a previous study of the activated sintering of M3/2 [12–15]. These mixtures with 10 vol % added ceramic powders were blended for 15–30 min in a conventional "TURBULA" system.

For both isothermal and gradient-furnace sintering experiments, cylinders 10 mm diameter and about 8 mm deep were uniaxially cold-pressed (under 750 MPa in a floating die arrangement). For gradient-furnace sintering these cylinders were bored before piling them up on an alumina tube which contained a thermocouple (Fig. 2). One parallelepiped sample of M3/2 + Cu_3P without ceramic addition was cold pressed at 600 MPa, sintered 1 h at 800 °C, and machined as a cylinder 9 mm diameter and 85 mm high.

Isothermal sintering experiments were carried out at 1150 °C for 30 min under primary vacuum. The samples were furnace cooled. For gradient-furnace sintering, the furnace was preheated before the introduction of the pile of samples in the gradient zone under primary vacuum. This temperature gradient was controlled during sintering. After 75 min the samples were quenched in a water-cooled box.

2.3. Characterization

Reactions occurring during the sintering of mixtures were detected using a SETARAM TGDTA 92 differential thermal analyser operating in a dynamic atmosphere of argon and using alumina as a reference material. Quantitative image analysis (QIA) was carried out using a NORAN TN 8502 image analyser, which was directly connected to an optical microscope (using a camera), or to a scanning electron microscope (SEM, Philips 501).

Complementary to SEM observations, interfaces were observed with a 300 kV transmission electron microscope (TEM, Philips EM 430). Thin foils were obtained by mechanical polishing up to 100 μm, dimple grinding up to 30 μm, and ion milling.

Wear properties were studied using a pin-on-disc tribometer. A load of 5 N was applied on a grey iron pin. The velocity of the disc (tested material) was 0.1 $m\,s^{-1}$ at the contact point. The friction coefficient was monitored during the whole test. The wear rate was calculated using the conventional expression

$$\text{wear rate } (mm^2\,N^{-1}) = \text{material loss } (mm^3)/\text{contact energy } (N\,mm^{-2}) \quad (1)$$

Volume loss of the disc was measured using radial rugosimeter profiles, and that of the pin by measuring the wear facet.

3. Microstructures

3.1. Microstructural evolution during sintering

[M3/2 + 7 wt % Cu_3P + 0.25 wt % C] without ceramic addition, with 10 vol % TiN-coated Al_2O_3 and 10 vol % TiC were sintered in a gradient furnace. In the two piles of composites, the cylinders would not "glue" to each other during sintering: no liquid phase migrated between the different parts.

Porosity was measured along a polished axial section of the samples. Series of adjacent images were acquired with an optical microscope for the base material and for the material with TiC additions, and using SEM for TiN-coated Al_2O_3 additions which

TABLE II Characteristics of powders and ceramics used

	Mean particle size (μm)	Specific area (measured by BET) (m^2g^{-1})	Hardness (HV) [22, 23]	Wetting angle by Fe–P-C eutectic melt at 1280 °C [3] (deg)
Al_2O_3	40–50	0.165	1350–2250 depending on orientation	92
TiN-coated Al_2O_3	40–50 (mean TiN thickness: 200 nm)	0.065	TiN: 1800–2100 depending on stoichiometry	On TiN 33
TiC	30–60 (gradient furnace sintering) or 5–25 (isothermal sintering)	0.151 (30–60 μm powder)	1500–3200 depending on stoichiometry	32

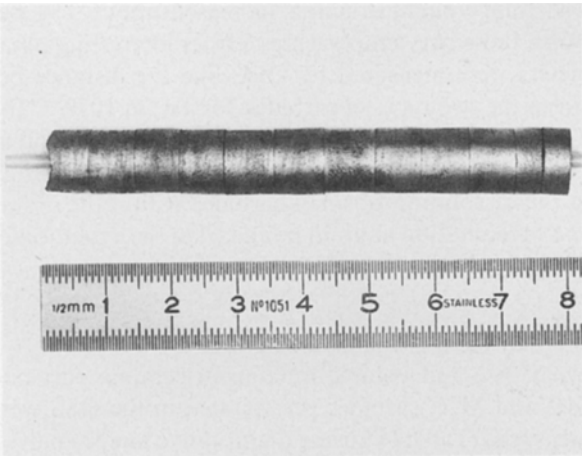

Figure 2 Optical image of a sintered pile of samples (M3/2 + 7 wt % Cu_3P + 0.25 wt % C) + 10 vol % TiC.

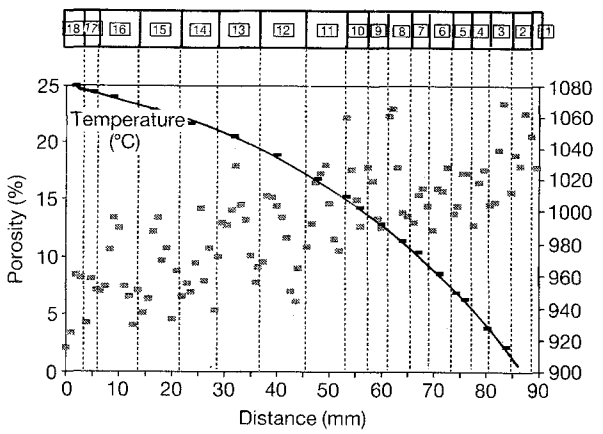

Figure 3 Porosity measured by QIA along a stack of composite cylindrical samples containing TiN-coated Al_2O_3. Samples sintered in a gradient furnace. The temperature gradient is also plotted.

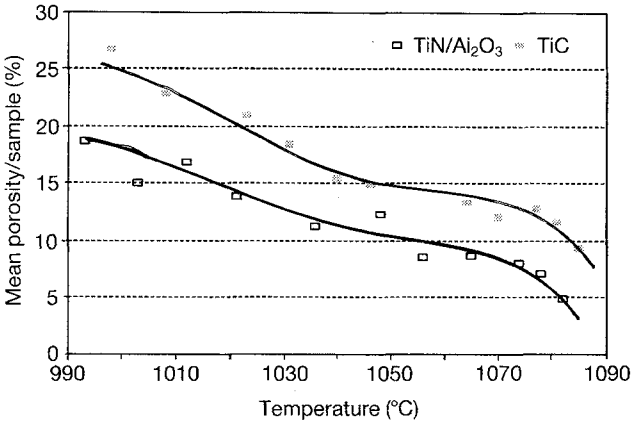

Figure 4 Mean porosity per sample along a stack of cylindrical samples of TiN-coated Al_2O_3 and TiC composites sintered for 75 min.

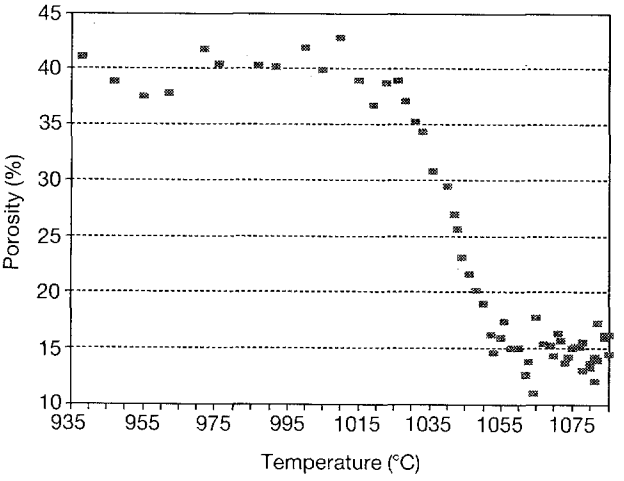

Figure 5 Porosity along a monolithic sample without ceramic addition sintered for 75 min.

needed a better contrast. In the composites, graphs exhibiting the same shape (e.g. Fig. 3) showed that porosity was more important in the middle of each elementary sample of the pile. This was interpreted as an effect of the uniaxial cold compaction before sintering. The smallest samples of these piles did not present this particularity because they were produced by cutting the largest into two parts before sintering (samples 1–10 of TiN-coated Al_2O_3 composite, for instance). However, the decrease of porosity with increasing sintering temperature was significant, as might be better shown by the graph (Fig. 4) which gives the mean porosity per elementary sample of the piles. The porosity graph of the base material was more continuous, because of the use of a monolithic sample (Fig. 5).

For the three mixtures, densification proceeds in two steps, the beginning of which corresponds to the apparition of liquid phases, as ascertained by the DTA thermograms presented in Fig. 6: Fe–M_3P carbides

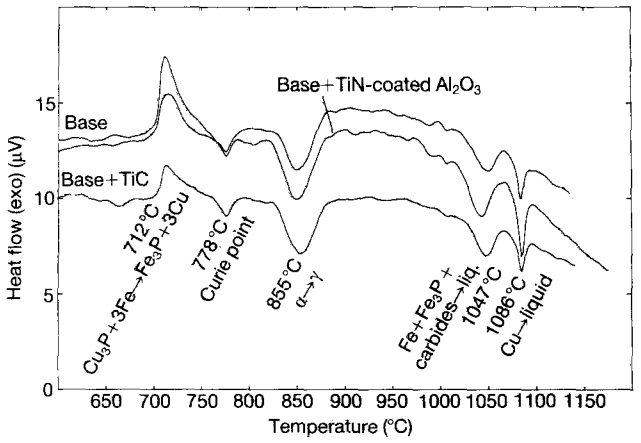

Figure 6 DTA thermograms of (M3/2 + 7 wt % Cu_3P + 0.25 wt % C) pure, + 5 wt % TiC, + 5 wt % Al_2O_3, and + 5 wt % TiN-coated Al_2O_3.

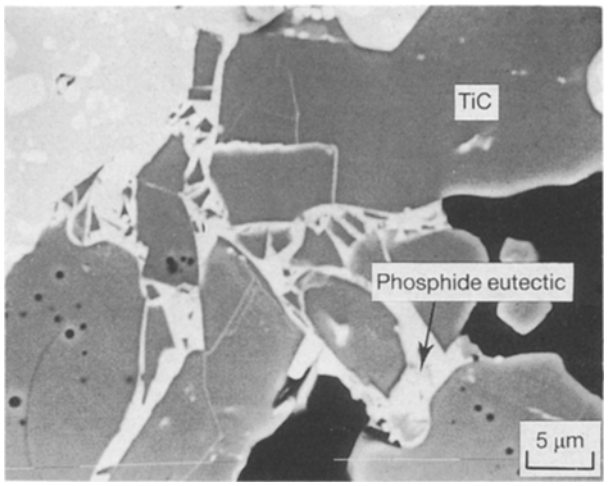

Figure 7 SEM image of (M3/2 + 7 wt % Cu_3P + 0.25 wt % C) + 10 vol % TiC at 1010 °C.

eutectic melting begins near 1000 °C (maximum at 1047 °C for the composites and 1043 °C for the base material without addition) and copper melting at about 1070 °C (maximum at 1086 °C). TiC composite was the least densified material.

The TiC particles were broken during cold compaction of the samples as ascertained by observations of the mixtures before and after applying the 750 MPa. This is probably due to their complex shape (Fig. 1) in addition to their fragility. Micrographs of the samples treated in the gradient furnace showed that the eutectic melt penetrated inside these broken particles as soon as it was melted (Fig. 7).

The observation of these samples at a higher magnification using SEM and QIA gave information on the size and volume fraction of primary carbides (MC with M = primarily V, Cr and M_6C with M = primarily Fe, W, Mo) in the matrix at various temperatures: an example is given in Table III for the TiC-containing composite. The minimal number of treated images was calculated according to the magnification used and the size of the measured phases. In case of carbides, for a magnification of 1250, 25–30 images were sufficient for a good accuracy. The mean size of M_6C carbides doubled between 1025 and 1150° C, while the mean size of MC remained much the same. The total volume fraction increased about 3 % between these two temperatures. Other interesting parameters were measured by QIA, like the distance between the two types of carbides: for TiC at 1070 °C the distribution of M_6C was uniform in the grains, and at 1080 °C a second population appeared corresponding to the dissolution of small carbides within the grains and precipitation at grain boundaries; the evolution of the MC population was less marked.

3.2. Sintered microstructures

Mean size and volume fraction of ceramic particles, MC and M_6C carbides precipitated in the HSS were measured (Table IV) using quantitative image analysis of secondary or backscattered electron images of composite samples which had been sintered for 30 min at 1150 °C under a primary vacuum (microstructures in Fig. 8). The actual size of the ceramic added differed from the nominal size (Fig. 9a). This could be explained by the fact that the techniques used to measure the particle size are generally less sensitive than QIA. For example, laser granulometer measurements assume that particles are spherical: Fig. 9b shows results for alumina powders. In case of TiC particles, the difference with nominal particle size is also due to the breakage of particles during cold compaction, mentioned above.

For uncoated alumina, pores were observed at the interfaces and between particles. For TiN-coated

TABLE III Mean size and volume fraction of carbides in a TiC-containing composite. (The volume fractions are given relative to the total area of the images)

	Temperature and distance			
	1025 °C 60 mm from the top	1070 °C 21 mm from the top	1080 °C 3 mm from the top	1150 °C sintered sample
Number of images (magnification)	25 (× 1250)	30 (× 1250)	30 (× 1250)	40 (× 1250)
M_6C mean size (μm)	0.7 ± 0.2	0.7 ± 0.2	1.0 ± 0.2	1.4 ± 0.3
M_6C vol. fraction (%)	6.9 ± 0.4	7.9 ± 0.4	8.2 ± 0.4	8.9 ± 0.4
MC mean size (μm)	1.0 ± 0.2	1.1 ± 0.2	1.2 ± 0.2	1.3 ± 0.2
MC vol. fraction (%)	3.2 ± 0.2	3.6 ± 0.2	4.7 ± 0.2	4.4 ± 0.2

TABLE IV QIA results for samples sintered for 30 min at 1150 °C under vacuum and furnace cooled

		Without ceramic addition	HSS + Al_2O_3	HSS + TiN-coated Al_2O_3	HSS + TiC
Number of treated images (magnification)		30 (× 1375)	5 (× 160) and 40 (× 1250)	5 (× 160) and 32 (× 1250)	40 (× 1250)
M_6C	mean size (μm)	2.6 ± 0.5	1.5 ± 0.4	2.1 ± 0.3	1.4 ± 0.3
	(vol %)	14.6 ± 0.4	11.6 ± 0.4	11.4 ± 0.4	8.9 ± 0.4
MC	mean size (μm)	2.2 ± 0.5	1.3 ± 0.4	1.5 ± 0.2	1.3 ± 0.2
	(vol %)	3.3 ± 0.2	3.8 ± 0.2	3.7 ± 0.35	4.4 ± 0.2
Ceramic	mean size (μm)	–	50 ± 0.5	53 ± 0.5	16 ± 0.5
	(vol %)	–	8.6 ± 0.2	8.6 ± 0.2	9.0 ± 0.2
Residual porosity (%)		1.2	1.6	0.6	0.6 – 1.2 (insufficient contrast)

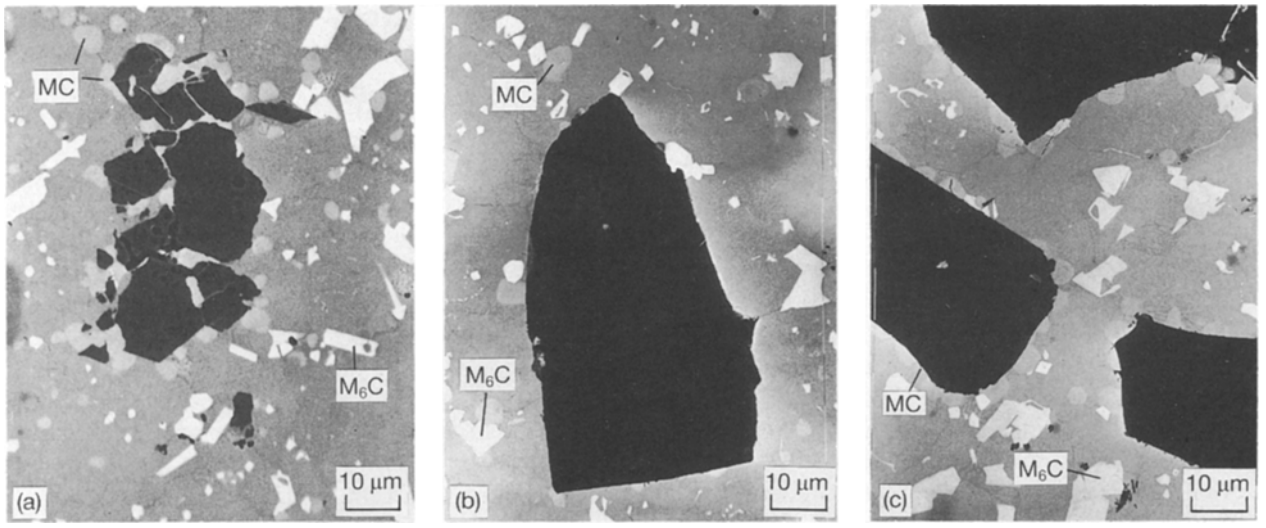

Figure 8 SEM images of composites sintered 30 min at 1150 °C in vacuum. (a) TiC, (b) Al_2O_3, (c) TiN-coated Al_2O_3.

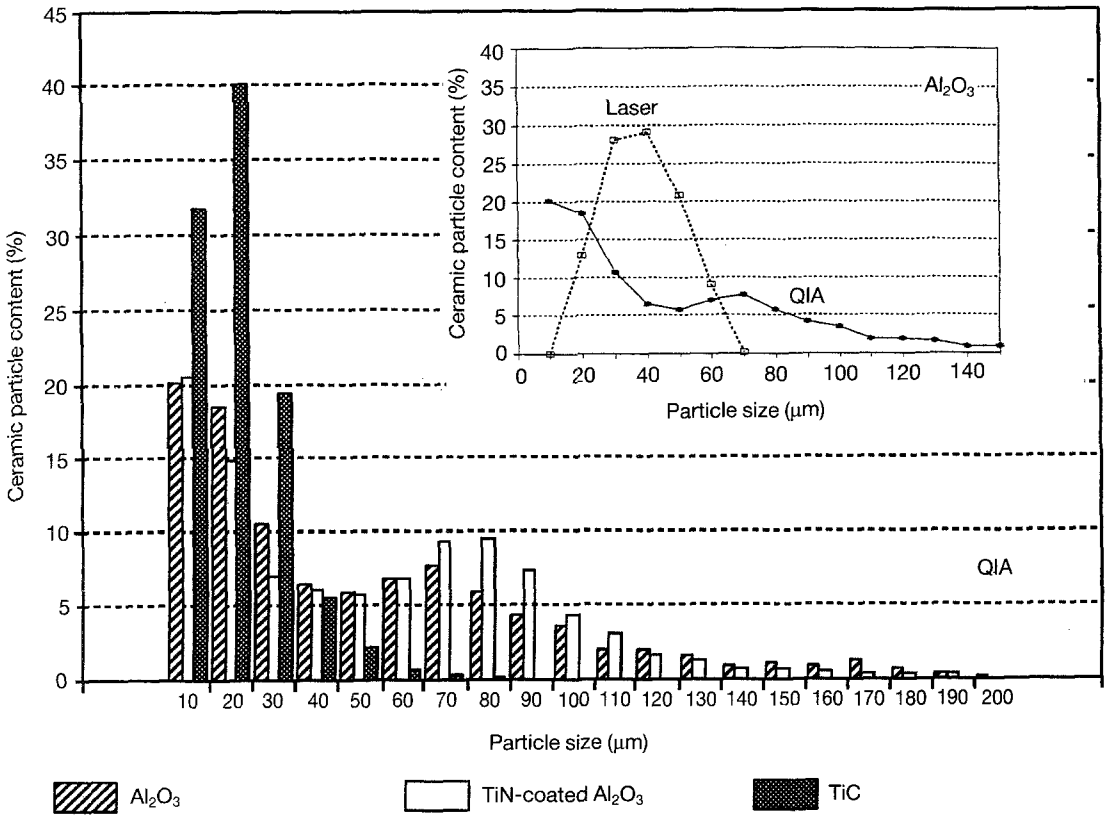

Figure 9 Size of the ceramic particles measured by QIA and laser granulometre.

Al_2O_3 and TiC additions, no porosity was observed at the ceramic/matrix interfaces, but a preferential precipitation of MC was noted (Fig. 8). QIA results (Table IV) showed that ceramic addition decreased the mean size of the carbides and increased the MC/M_6C ratio. In TiN-coated Al_2O_3 composite this MC/M_6C ratio remained the same as for the composite containing Al_2O_3, but the ratio increased for TiC addition.

Images of the interfaces on a finer scale, obtained by TEM, showed an M_3P phosphide phase containing MC and M_6C precipitated carbides all along the TiC and TiN interfaces and in very fine capillary formed by the broken particles (Fig. 10). The presence of these carbides in these sites indicates that they were involved in the first stage of densification due to the eutectic melting [12–15]. For uncoated alumina no phosphide layer but much porosity at the interfaces was observed. These observations confirmed the importance of the wetting behaviour of the phosphide eutectic melt against the ceramic particles for the densification of the composites and the particle/matrix cohesion.

4. Wear test results

Increased wear resistance of reinforced HSS was noted (Fig. 11): the wear track of the composite discs was very low. The highest wear rate was obtained for those containing TiC. The value of the friction coefficient, after a quick removal of the superficial pollution layer, remained constant throughout the whole test, and was virtually identical for all the materials: about 0.8.

The metallic matrix (martensite + residual austenite + primary carbides) did not exhibit severe degradation. Composite materials showed two different aspects. The worn surface of the TiC-reinforced material appeared to be similar to the unreinforced material (Fig. 12a) and TiC particles did not seem to play any particular role in the protection of the matrix. On the other hand, both uncoated and TiN-coated Al_2O_3 particles were shown to protect the matrix because they are preferential sites for the formation and accumulation of debris (Fig. 12b). X-ray diffraction analysis showed that this debris was Fe_2O_3 containing very fine particles of TiC and Al_2O_3 in the case of composites.

5. Discussion

The sintering of samples in a furnace with a temperature gradient allowed observation of the behaviour of liquid phases against ceramic particles during sintering. The TiC particles broken during compaction were wetted and penetrated by the $Fe–M_3P$ carbides eutectic as soon as it melted. This phenomenon decreased the amount of liquid phase in the matrix and thus decreased the rate of densification comparing to TiN-coated Al_2O_3 particles where the interface area wet was much smaller, because these particles were not broken during compaction. This is an indication that, as for base material sintering [15], the first important stage of sintering is a mechanical rearrangement of the particles.

The use of a pile of small samples for sintering in this gradient furnace in the case of composite materials allowed us to verify that the liquid phases formed during sintering did not diffuse all along the sample. But for a small amount of liquid phase, as in this case, the use of a monolithic sample (as used for the base

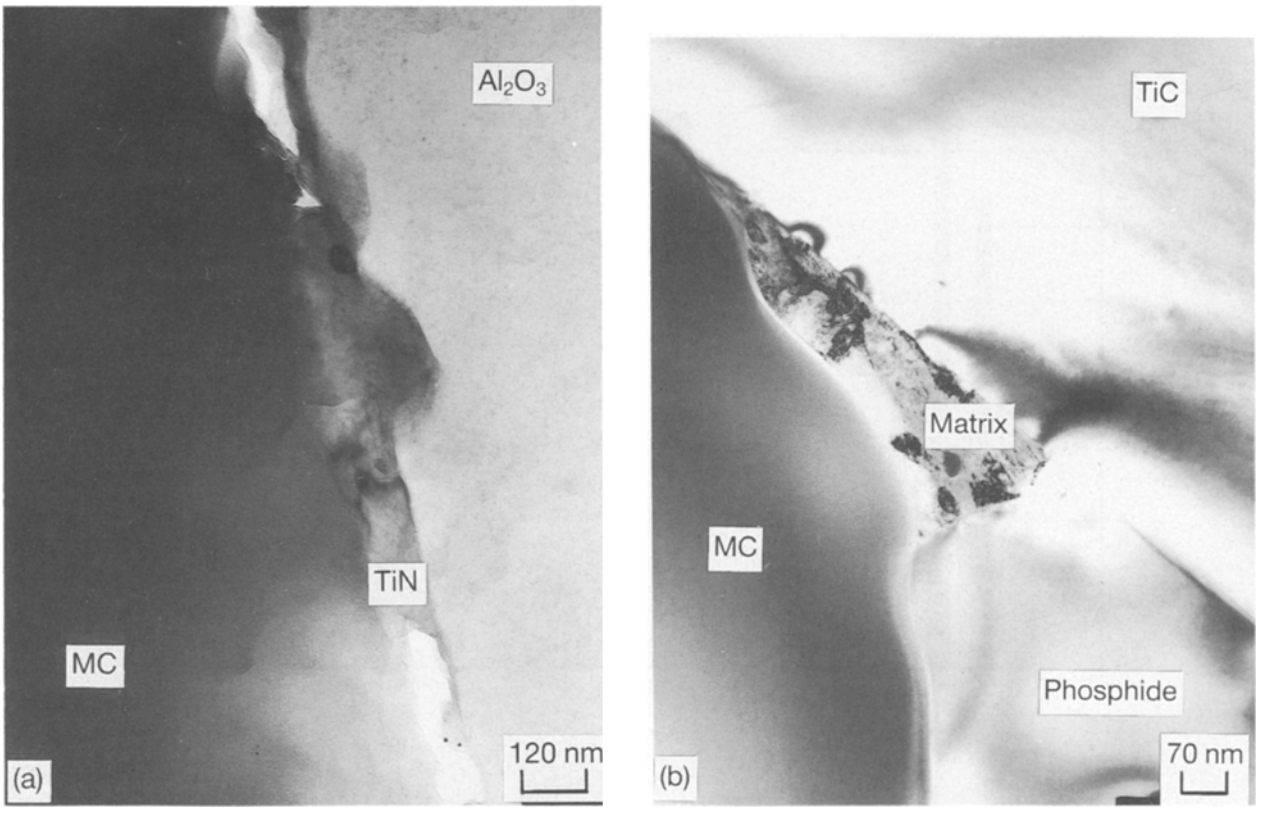

Figure 10 TEM images of TiN-coated (a) Al_2O_3 and (b) TiC interfaces with the matrix.

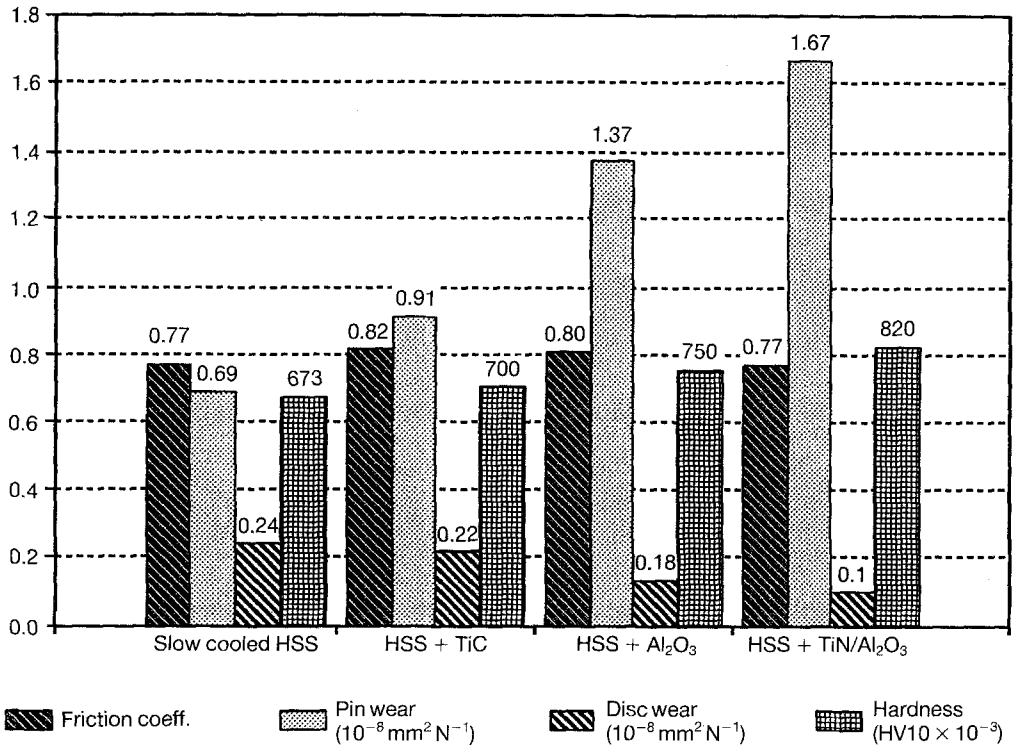

Figure 11 Pin-on-disc wear results.

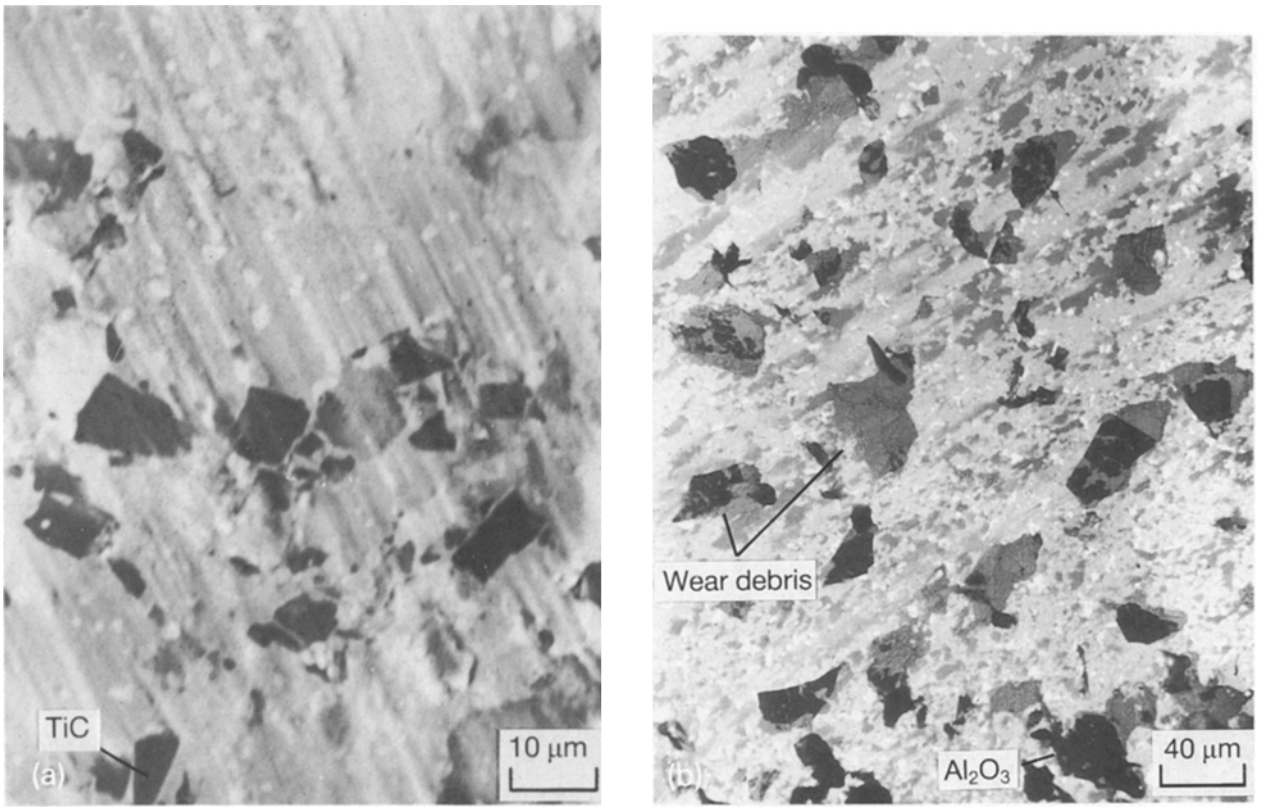

Figure 12 SEM images of the surface after pin-on-disc test. (a) TiC-containing material, (b) TiN-coated Al_2O_3 containing material.

material sintering) gives a more homogeneous green structure and thus the evolution of microstructure was continuous and representative of the temperature influence (Fig. 5)

Using the same sintering parameters, the addition of ceramic particles wet by the phosphide eutectic (TiC, TiN) led to a higher densification with 0.6% residual porosity. In the case of unwet ceramic particles, like uncoated Al_2O_3, 1.6% residual porosity was found. This influenced the wear test results: wear resistance was higher for the TiN-coated alumina than for uncoated alumina-containing materials. This increase of wear resistance was certainly not only due to the decrease of porosity but also to a higher cohesion between the particles and the matrix. This cohesion was due to the reactivity between the two phases

which promoted wetting. This effect is the object of further studies at the Centre des Materiaux de l'Ecole des Mines de Paris [24].

The addition of ceramic particles to the matrix increased the precipitation of MC carbides (which have a higher hardness than the M_6C): without ceramic addition the MC/M_6C ratio was 0.2, on adding alumina particles (coated or uncoated) it was 0.3 and on adding TiC particles it reached 0.5. For TiN-coated Al_2O_3 particles, a preferential precipitation of MC at the interface occurred as for TiC particles, but the total volume fractions of carbides was the same in the case of uncoated alumina particles composites.

The better wear behaviour provided by the Al_2O_3 particles compared with that provided by TiC particles, despite a lower hardness (Fig. 11) and the same volume fraction of the two ceramics, could be due to a higher mechanical strength and a lower toughness of the Al_2O_3 particles. It could also be due to the lower mean particle size of the TiC addition, decreased by the breakage of these particles during cold compaction, while the Al_2O_3 particles were not broken and their mean particle size remained near 50 μm (Fig. 9). The role of cohesion between the ceramic particles and the metallic matrix, underlined in case of coated Al_2O_3 particles, appears to be a minor factor in this case, because TiC particles showed better cohesion with the matrix than the uncoated Al_2O_3 (which showed porosity at the interface).

6. Conclusions

1. The use of a temperature-gradient furnace allowed the study of the liquid-phase sintering of composite materials with a reduced number of experiments. The temperature control during sintering, coupled with the observation of axial section of the samples, gave a great deal of results related to the densification mechanisms of the materials. Quantitative image analysis proved to be a powerful tool to obtain elements for discussing these mechanisms.

2. The densification rate of the composite materials was governed by the interface area of ceramic particles with the matrix. Thus it is important to know the actual size of ceramic particles added: the breakage of TiC particles during cold compaction caused a large increase of this interface area. The Al_2O_3 particles, coated or uncoated, were not broken.

3. The volume fraction, hardness and reactivity of the ceramic phase were not the only parameters influencing the wear resistance. The residual porosity and the ceramic particles size must also be considered.

4. The TiN coating of the Al_2O_3 particles gave numerous advantages: the wettability by the liquid phases, therefore the cohesion with the matrix, was better and thus promoted the densification rate and the wear resistance. This coating process allowed regular-shaped and coarse ceramic particles to be obtained with the TiN properties at the surface, which was prominent because coarse pure TiN powder cannot be easily produced.

Acknowledgements

This work was undertaken through contract RI1B-0203 for the Commission of the European Communities under the BRITE programme for industrial research and development. TiN coating of alumina particles was performed by Xycarb BV (The Netherlands) which is gratefully acknowledged.

References

1. F. THÜMMLER and C. GUTSFELD, *Powder Metall. Int.* **23** (1991) 5.
2. S. J. YANKEE and B. J. PLETKA, *J. Mater. Sci.* **26** (1991) 5067.
3. C. ZHOU, J. R. MOON and S. PEACOCK, *Powder Metall.* **34** (1991) 1.
4. M. CHEN, T. Z. KATTAMIS, B. V. CHAMBERS and J. A. CORNIE, in "Proceedings of the Conference on Engineered Materials For Advanced Friction and Wear Applications", Gaithersburg, MD, 1–3 March 1988 (ASM, Materials Park, OH, USA, 1989) p. 63.
5. B. CHAMPAGNE, R. ANGERS and M. FISET, in "Proceedings of PM '84", Toronto, Canada, 11–12 June, edited by E. N. Aqua *et al.* (MPIF, Princeton, NJ, USA, 1985) p. 237.
6. M. PIERRONET, G. RAISSON, F. GAILLARD and J. L. HEUZE, in "Proceedings of Colloque sur les Materiaux à Propriétés Physiques Particulières Obtenus à Partir de Poudres", 6–8 April 1992, Paris, France (SF2M Publ., Paris, France, 1992) p. 30.
7. R. A. QUEENEY, R. E. MASTERS, R. J. BELTZ, and J. D. DANKOFF, *Mod. Devel. Powder Metall.* **20** (1988) 409.
8. R. A. QUEENEY, R. J. BELTZ and J. D. DANKOFF, in "Proceedings of Powder Metallurgy 90", London, Vol. 2, (Institute of Metals, London, 1990) pp. 107–12.
9. N. UCHIDA, and H. NAKARUMA, in "Proceedings of 12th International Plansee Seminar '89, High temperature and wear resistant materials in a world of changing technology", 8–12 May 1989, Reutte, Tirol, Austria, edited by H. Bildstein and H. M. Ortner, Vol. 2 (RWF Publ., Watters, Austria, 1989) pp. 541–55.
10. P. K. KAR and G. S. UPADHYAYA, *Steel Res.* **62** (1991) 352.
11. U. BRYGGMAN, J.-O. LINDQVIST, in "Proceedings of PM '92", San Francisco, USA (1992).
12. J. D. BOLTON, M. JEANDIN, and C. JOUANNY-TRESY, *Powder Metall.* **33** (1990) 126.
13. C. JOUANNY-TRESY, N. DE DAVE, M. JEANDIN and J. MASSOL, in "Proceedings of Colloque sur la Maîtrise des Matériaux Frittés par leur Microstructure", Paris, 19–21 March 1990, SF2M (1990) p. 14.
14. J. D. BOLTON and H. V. BAAH, *Powder Metall.* **34** (1991) 273.
15. J. D. BOLTON, A. J. GANT and R. J. M. HAGUE, *J. Mater. Sci.* **26** (1991) 5203.
16. J. D. BOLTON in "Proceedings of Colloque sur la maîtrise des propriétés des métaux frittés par leur microstructure", 19–21 March 1990, SF2M, Paris, France (1990) p. 15.
17. M. M. OLIVEIRA, *ibid.*
18. S. RUPP, Thèse de Docteur-Ingénieur, Ecole des Mines de Paris, 29 November 1986.
19. M. JEANDIN, S. RUPP, J. MASSOL and Y. BIENVENU *Mater. Sci. Eng.* **77** (1986) 139.
20. C. JOUANNY-TRESY and M. JEANDIN, in "Proceedings of Journées d'automne 1991", Paris, 8–10 October 1990 (SF2M, Paris, France, 1991).
21. C. JOUANNY-TRESY, P. VON ROSENTIEL, M. JEANDIN and M. DURAND, in "Proceedings of "EUROMAT '91"", Cambridge, UK, 22–24 July 1990 (Institute of Metals, London, 1991) B2b–p 7.
22. G. ALLIPRANDI, in "Matériaux réfractaires et céramiques techniques" (Septima, Paris, 1979).
23. J. L. CHERMANT, in "Les céramiques thermomécaniques", (CNRS, Paris, 1989).
24. C. JOUANNY-TRESY, Thèse de Doctorat, Ecole des Mines de Paris, December 1992.

Received 9 September 1992
and accepted 11 March 1993